

## Phase-field model: Boundary layer, velocity of propagation, and the stability spectrum

Raz Kupferman, Ofer Shochet, and Eshel Ben-Jacob

*School of Physics and Astronomy, Raymond and Beverly Sackler Faculty of Exact Sciences, Tel-Aviv University, Ramat-Aviv, Tel-Aviv 69978, Israel*

Zeev Schuss

*School of Mathematics, Raymond and Beverly Sackler Faculty of Exact Sciences, Tel-Aviv University, Ramat-Aviv, Tel-Aviv 69978, Israel*

(Received 11 June 1992)

We present a study of a phase-field model for diffusion-limited growth. A boundary-layer approximation is used to show that for sharp interface, the first approximation to the phase-field model is the free boundary model, which includes surface tension and a linear kinetic term. The velocity of propagation and the stability spectrum are calculated for a steady-state flat interface. In the case where the phase and the field have similar variation lengths, a stable growth regime is found above a critical value of driving force. We discuss the application of phase-field-like models in the description of the ensemble-average pattern.

### I. INTRODUCTION

Interfacial pattern formation in diffusion-limited growth has been the focus of extensive studies in the past decade.<sup>1-3</sup> At present, it is understood that the rich variety of patterns observed in different systems, such as solidification from supersaturated solution or from undercooled melt, is the reflection of a competition between a macroscopic driving force, such as gradients of concentration or gradients of temperature, on the one hand, and microscopic interfacial effects, such as surface tension, surface kinetics, and anisotropy, on the other hand. The microscopic effects, although relatively small, were found to be singular perturbations, playing a crucial role in the selection of the growth pattern. Powerful mathematical tools were developed in order to describe the interplay between the competing effects, resulting in the formulation of the microscopic solvability condition for dendritic growth.<sup>4-12</sup>

With the discovery of the microscopic solvability criterion, the consensus was that the problem of dendritic growth was finally solved. All the main results were obtained from the study of the free boundary model of solidification. This model approximates the system's dynamics by a single macroscopic diffusion field, whereas all the relevant microscopic dynamics is embodied in phenomenological boundary conditions at the interface. The solvability criterion states that for any set of parameters, *provided that anisotropy is present*, there exists only a discrete set of needlelike steady-state solutions, among which only the fastest is linearly stable. Therefore, it is predicted to be the one observed. An open question is how general these results are. Will the same selection mechanism hold if the dynamics depends on more than one field? Furthermore, what will happen if the phenomenological interfacial parameters are replaced by real mi-

croscopic kinetic rules? As mentioned above, even very small changes in interfacial kinetics can have strong effects on the dynamical behavior of the system, so that it is crucial to clarify these issues. Even if such a general selection mechanism exists, it is still necessary to construct a more microscopic picture. The purpose of such a picture is to understand how the microscopic kinetics influences the macroscopic level and to determine the relation between the parameters of the two levels.

A more profound problem is the fact that in numerical simulations, as well as in experiments, dendrites are not always observed, even if anisotropy is present. Instead, for a certain regime of parameters, the front undergoes repeated tip splitting.<sup>13-17</sup> Thus, the solvability criterion can clearly be only a part of the general picture, and a more general principle is needed to select between different growth forms.<sup>3,14,18</sup> Moreover, the solvability criterion is obtained by an asymptotic matching of the steady-state solutions at infinity. However, in experiments, the underlying needle crystal does not extend all the way to infinity. When the growth conditions are locally changed, the dendrite's tip immediately selects a new shape, independently of the matching to the remaining part of the structure.

Next, there is the question of how to extend the theory from describing the evolution of a single stem to the description of the global structure of the entire morphology. The microscopic solvability criterion refers only to the tip of an isolated needle crystal. Real dendrites are far from being just a needle crystal. They look more like a "backbone" decorated with a complex of well-developed sidebranches.<sup>19</sup> In addition, the stable phase forms many dendrites growing in a self-organized manner, to form the global structure—the morphology. Similarly, tip-splitting growth is only a basic element of the growth process that leads to the formation of the

dense-branching morphology.<sup>3,20,21,22</sup>

One strategy towards answering these outstanding questions is to study phase-field-like models.<sup>23,24</sup> Such models consist of a diffusion equation coupled to a time-dependent Ginzburg-Landau equation for an order parameter (the phase) of the system. The phase-field approach can be considered a more detailed model than the free boundary model, the latter being a limiting case for a very sharp interface in the former. A study of the phase-field model can show if a generalization of the microscopic solvability criterion applies to a wider class of models. It is not *a priori* obvious that a similar mechanism acts in this case. In the free boundary model, the boundary conditions are the reflection of a second field (the phase), so that the singular nature of these conditions is natural. In the case of a phase-field model, the situation is different. For example, surface tension is inherent in the phase-field model; hence, it has no meaning to refer to a model with or without surface tension. On the other hand, the inclusion of anisotropy is easily understood to act as a singular perturbation, as it is incorporated into the model by replacing the Laplacian operator in the phase equation by a higher-order operator.<sup>25</sup>

The importance of the phase-field model, as a generalization of the free boundary model, motivated a large number of analytical and numerical studies. Collins and Levine<sup>26</sup> were the first to apply it in the description of solidification from undercooled melt with a diffuse interface. They showed the existence of a solvability condition for the steady-state velocity of a flat interface for a continuous range of undercooling. This provided a first link between the phase-field model and the free boundary model with a kinetic term. Langer<sup>27</sup> derived the relations between the parameters of the two models using qualitative arguments. The mathematical foundation of these relations was given by Fife and Caginalp,<sup>28–30</sup> who derived the free boundary model from a phase-field model in the limit of a sharp interface using a boundary-layer approximation. Liu, Mondello, and Goldenfeld<sup>31</sup> studied a phase-field model for the time evolution of a superconductor following a quench from a normal state, where the order parameter is a complex field. They showed the analogy between this case and solidification from undercooled melt by approximating this problem by a free boundary model and thus identifying the stabilizing and destabilizing mechanisms at the interface.

Numerical simulations of the phase-field equations were performed by Fix and Lin,<sup>32</sup> Lin,<sup>33</sup> and more recently by Kobayashi,<sup>34</sup> who also performed three-dimensional (3D) simulations.<sup>35</sup> These simulations gave results in qualitative agreement with simulations of the free boundary model.<sup>36</sup> Frahm, Ullah, and Dorsey<sup>27</sup> simulated the normal to superconducting transition with a complex order parameter and obtained tip-splitting growth.

We have it in mind to use the phase-field approach in a different context, motivated by recent results,<sup>21,38</sup> showing that for both dendritic morphology and for the dense-branching morphology, growth is within a well-defined shape-preserving envelope, in agreement with previous predictions.<sup>18,20,22,39</sup> A natural approach is to describe the propagation of this envelope as the penetra-

tion of a “stable phase,” that is, the solid-liquid mixture, into a metastable one—the solution. Noting that the two characteristic length scales, the diffusion length and the thickness of the envelope, may be of the same order of magnitude, it seems that a phase-field-like model would be a more appropriate way to describe the dynamics of the envelope (this issue will be discussed in detail in Sec. II) than a free boundary model with a sharp interface. It is still not completely clear, yet, what the relevant fields and the effective parameters which govern the growth of the envelope are. However, before performing such a modeling, a fundamental question has to be set: Can the same model describe for one regime of parameters a solid-liquid interface in which interfacial instabilities develop complex patterns, whereas for another regime of parameters it produces a stable and shape-preserving pattern.

In Sec. III we present the phase-field model. We write the final equations in a dimensionless form, where the length and time units depend on a characteristic velocity in the phase equation. The model includes three dimensionless parameters. In Sec. IV we derive the free boundary model which contains surface tension and surface kinetics as a leading-order approximation to the solution of the phase-field model. To this end, we introduce a scaling parameter, which depends on a characteristic velocity of the problem which we identify. This analysis gives an additional insight into the role of surface tension and surface kinetics as singular perturbations. Specifically, it is found that although surface tension scales like the small parameter of the asymptotic expansion, it appears in the leading-order term of the reduced model. This analysis differs from that of Refs. 28–30 in the fact that, there, the boundary terms appear only in the second term of the expansion, whereas the first term satisfies the Stefan problem. Thus, the patterns formed by the leading-order term can be very different from those formed by the second term. It follows that the effects of surface tension and linear surface kinetic corrections are scaled by the expansion parameter and become negligible in the asymptotic limit, contrary to the numerically and experimentally observed evidence. In Sec. V we review, for completeness, the one-dimensional steady-state problem, which corresponds to the expansion of a flat interface in higher dimensions.<sup>40</sup> We write a solvability condition for the steady-state velocity and compare the results to the predictions of the free boundary model in the appropriate limit. In Sec. VI we study the linear stability of the steady-state solution of a flat interface. For the case of sharp interface, we retrieve the stability spectrum of the free boundary model. The wavelength of the marginally stable mode is found to be shorter the sharper the interface is; hence, the interface develops instabilities with very large curvatures. It explains why the product of surface tension, which is proportional to the thickness of the interface, and the curvature of the interface remains a quantity of order 1, even in the limit of vanishing surface tension. In this limit, the interface is linearly unstable for all values of driving force. In the opposite limit, where the two fields have similar characteristic lengths, above a critical value of driving force, the interface becomes

stable against perturbations of all wavelengths. Finally, in Sec. VII we summarize the results and suggest their applications to future studies.

## II. MOTIVATION: SHAPE-PRESERVING ENVELOPE OF ENSEMBLE AVERAGING

In this section we review recent results of morphology transitions in diffusion-limited growth, in systems described by a conserved order parameter such as the concentration field in solidification from a supersaturated solution.<sup>21,22,38,41,42,43</sup> These results provide the main motivation for studying the phase-field model as a means for describing envelope growth. The study<sup>21,38</sup> was based on a new numerical scheme, the diffusion-transition scheme, which is a hybridization of a continuous and an atomistic approach. It allowed us to study the different morphologies, to characterize them by the geometrical properties of their envelope, and to study the nature of morphology transitions.

For both dendritic morphology and the dense-branching morphology (DBM) it was found that the late-stage spatial dimension of the growing patterns was  $d = 2$ . The ensemble-averaged envelope is shape preserving, and propagates at constant velocity. For both morphologies, the envelope shows a pronounced fourfold symmetry, convex for DBM and concave (at  $45^\circ$  of the main growth directions) for dendritic growth (Fig. 1).

These results suggest the possibility of considering the propagation of the ensemble-averaged envelope as the propagation of an interface with an effective diffusion dynamics, surface tension, surface kinetics, and anisotropy (see Fig. 2).<sup>22</sup> Here, the stable phase is not pure solid but

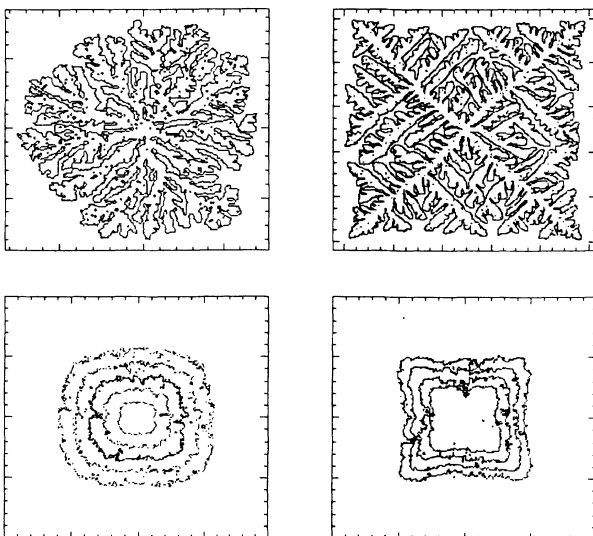


FIG. 1. (a) Typical realization of dense-branching growth. (b) Typical realization of dendritic growth. (c) Time sequence of an ensemble-averaged envelope of dense-branching growth over 30 different realizations. The envelope is shape preserving, convex, and shows a pronounced fourfold symmetry. (d) Time sequence of an ensemble-averaged envelope of dendritic growth. In this case, the envelope is concave.

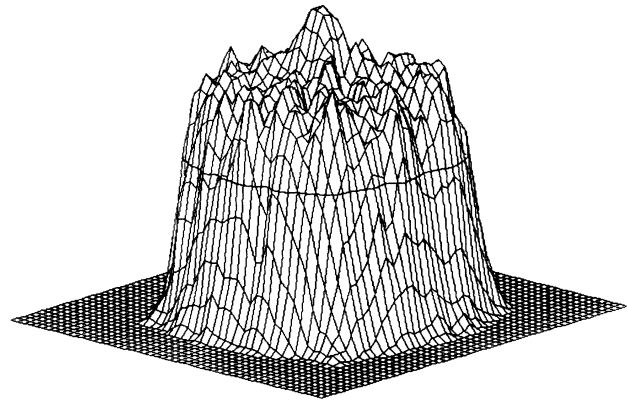


FIG. 2. Three-dimensional plot of the ensemble-averaged density of solid. The envelope is defined to be the 0.5 contour line. The higher averaged concentration at the center reflects the initial conditions, and the transient to steady state.

rather a mixture of solid and solution. This phase is not in equilibrium, but all the relaxation processes, due to surface tension, occur on a much longer time scale than the propagation of the front. Since the velocity of the envelope is constant, growth is not limited by diffusion from parts away from the interface. It implies that each realization grows with an average density of matter equal to the solution concentration far from the solid, which corresponds to unit supersaturation in solidification.<sup>44</sup>

Additional insight into the morphology dynamics is gained by considering Fig. 3. At the top it shows tip-splitting growth in a channel geometry. Below are the

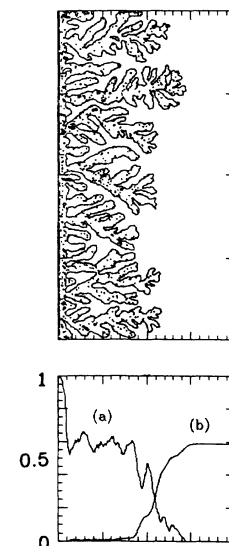


FIG. 3. Simulation results of the diffusion-transition scheme for growth in a channel. Top: Tip-splitting growth of fingers. Bottom: The average over the  $y$ -direction concentration of (a) solid and (b) liquid. The concentration of matter in the mixed phase is approximately equal to the liquid concentration at the right boundary. The decay lengths of both averaged solid and liquid concentrations is of the same order of magnitude.

averaged solid and liquid densities across the channel, which are similar to the ensemble averaging (for a sufficiently wide channel). The total concentration of matter behind the propagating front, is equal to the concentration in the liquid phase. Note that the two fields have decay lengths of the same order of magnitude, so that the interface is not sharp. Figures 2 and 3 suggest that a more appropriate description for the evolution of the ensemble-averaged envelope would be a phase-field-like model with an interface of finite width rather than a free boundary model, where the thickness of the interface is infinitely sharp.<sup>22</sup> Such an approach was recently applied successfully for the description of an ensemble-averaged diffusion-limited aggregation (DLA) growth.<sup>45</sup> At present, it is not clear which physical quantities correspond to the phase and to the field. We expect that these fields are not merely the averaged concentrations of solid and liquid (as in mean-field DLA), but rather contain more information, such as the characteristic widths of individual branches, the spacing between them, local orientation, etc.

The present paper provides the necessary infrastructure towards the development of a phase-field model to describe the ensemble dynamics. To this end, we first have to calculate the interface velocity and its stability spectrum as functions of the model's parameters. The next step will be to compare the results with those obtained in numerical simulations of the diffusion-transition scheme. Note that the simulations consider a conserved field, whereas the phase-field model describes a nonconserved order parameter.

### III. DESCRIPTION OF THE MODEL

In this section we present the phase-field model for a stable phase penetrating a metastable one. We consider the case where the phase of the system can be described by a single-component real order parameter  $\phi$ . The relative stability of the two phases varies as a function of a second parameter,  $u$ . For a given value of  $u$ , we denote the thermodynamical locally stable states of the system by  $\phi_-(u)$  (the "ordered" state) and  $\phi_+(u)$  (the "disordered" state). The intermediate states that lie in between are outside the scope of thermodynamics, so that the introduction of the concept of an order parameter is necessary for the analytical continuation of the thermodynamical quantities between the two stable states. For example, considering the liquid-solid transition in a pure substance, the order parameter can be identified with the specific entropy  $s$ , whereas  $u$  corresponds to the temperature field. For fixed temperature, the system has two local equilibrium states, solid and liquid, which differ in their specific entropies. The order parameter is a quantity which assumes values between the two equilibrium values of  $s$ .

Next, a free energy for homogeneous systems,  $F(\phi, u)$ , is introduced. The function  $F$  is also an extension of the equilibrium free energy and, as such, cannot be derived from any fundamental principles. However, as shown below, most of our results are not affected significantly by the exact functional form of  $F$ . For historical reasons,

the canonical choice for  $F$  is the  $\phi^4$  Ginzburg-Landau potential<sup>23</sup>

$$F(\phi, u) = (\phi^2 - 1)^2 - \lambda u \phi, \quad (3.1)$$

where  $\lambda$  is a positive coupling constant. Another common choice which was found to be convenient for numerical simulations is

$$F(\phi, u) = \ln[\cosh(\phi)] - \lambda u \phi \quad (3.2)$$

(Ref. 46). The piecewise parabolic potential

$$F(\phi, u) = \frac{1}{2}[\phi - \text{sgn}(\phi)]^2 - \lambda u \phi \quad (3.3)$$

(Ref. 40) was found to be convenient for analytical treatment and is used here. In this case, the local equilibrium states of the system, for a given  $u$ , are given by

$$\phi_-(u) = -1 + \lambda u, \quad \phi_+(u) = 1 + \lambda u. \quad (3.4)$$

We are interested in nonhomogeneous situations where the value of the order parameter is spatially variable. It is assumed that the total free energy of the system includes additional terms related to these spatial variations. If  $\phi(x)$  is a smooth function, the lowest-order derivatives dominate the free energy. For an isotropic system, a free-energy functional of the following form is proposed:<sup>23</sup>

$$\mathcal{F}[\phi] = \int_V dx \left[ \frac{1}{2} \xi^2 |\nabla \phi|^2 + F(\phi, u) \right], \quad (3.5)$$

where  $\xi$  is the characteristic variation length of  $\phi$ .

To study the time dependence of  $\phi$ , its dynamics has to be specified. In general, it is assumed that macroscopic systems undergo an overdamped motion towards equilibrium, that is, the free energy is monotonically decreasing in time. A simple equation satisfying this condition is the time-dependent Ginzburg-Landau equation

$$\tau \frac{\partial \phi}{\partial t} = - \frac{\delta \mathcal{F}[\phi]}{\delta \phi(x)}, \quad (3.6)$$

where  $\delta$  denotes a functional derivative and  $\tau$  is the characteristic relaxation time of the order parameter. Note that  $\tau$  is not derived from the free energy, unless the fluctuation-dissipation principle is assumed.<sup>47</sup> Combining Eqs. (3.3), (3.5), and (3.6), the phase equation

$$\tau \frac{\partial \phi}{\partial t} = \xi^2 \nabla^2 \phi + f(\phi, u) \quad (3.7)$$

is obtained, where

$$f(\phi, u) \equiv - \frac{\partial F(\phi, u)}{\partial \phi} = -\phi + \text{sgn}(\phi) + \lambda u. \quad (3.8)$$

The field  $u$  is assumed to satisfy a diffusion equation. The coupling between the dynamics of  $u$  and the dynamics of  $\phi$  is expressed by a source term in the diffusion equation. In solidification, this term corresponds to latent heat, which is the change in the specific entropy during the transition. The strength of the source is taken to be the time derivative of the order parameter,

$$\frac{\partial u}{\partial t} = D \nabla^2 u - \frac{1}{2} \frac{\partial \phi}{\partial t}, \quad (3.9)$$

where  $D$  is the diffusion coefficient, which is assumed symmetric on both sides. An additional parameter in the problem is the value of  $u$  in the metastable phase, which is a measure of the driving force in the process. We consider the case where the disordered phase is the metastable one and denote by  $-\Delta$  the value of  $u$  in this phase far from the interface.

The phase equation (3.7) defines a characteristic length scale  $\xi$  and a characteristic time scale  $\tau$ . In the field equation (3.9) they are combined in the diffusion constant  $D$ . To obtain the characteristic decay length of  $u$ , the diffusion length, we note that the source term in the field equation is proportional to the normal velocity of the interface  $v$ , so that the diffusion length is given by  $l = D/v$ . The ratio  $\xi/\tau$  is a characteristic velocity which is related to the kinetics of phase transition at the interface; hence,

$$l_k = \frac{D\tau}{\xi} \quad (3.10)$$

is a characteristic scale for the kinetics-limited diffusion length. Note that  $l_k$  is always shorter than  $l$ .

For convenience we define the following dimensionless coordinates: Length is measured in units of the diffusion length  $l_k$  and time in units of the corresponding diffusion time  $l_k^2/D$ , that is,

$$t \rightarrow (l_k^2/D)t, \quad x \rightarrow l_k x. \quad (3.11)$$

With these variables the dimensionless phase-field model is given by

$$\frac{\partial u}{\partial t} + \frac{1}{2} \frac{\partial \phi}{\partial t} = \nabla^2 u \quad (3.12)$$

and

$$\epsilon \frac{\partial \phi}{\partial t} = \epsilon^2 \nabla^2 \phi + g(\phi) + \lambda u, \quad (3.13)$$

with the boundary conditions  $u \rightarrow -\Delta$  and  $\phi \rightarrow \phi_+(-\Delta)$  as  $|x| \rightarrow \infty$  and given initial conditions  $u(x,0)$ ,  $\phi(x,0)$ . Here,  $g(\phi) = f(\phi,0)$ , and the parameter

$$\epsilon \equiv \frac{\xi^2}{D\tau} = \frac{\xi}{l_k} \quad (3.14)$$

is the ratio of the characteristic decay lengths of  $u$  and  $\phi$ , respectively. It is also the ratio of the diffusion coefficients in (3.7) and (3.9). Note that the height of the potential barrier can be normalized to 1 by an appropriate rescaling of the fields.

#### IV. THE LIMIT OF A SHARP INTERFACE: THE EFFECTIVE SURFACE TENSION AND SURFACE KINETICS

In many physical applications the characteristic scales of the two fields differ by several orders of magnitude. For example, in solidification from undercooled melt, the thickness of the interface is only a few atomic layers wide, whereas the thermal diffusion length is typically of the order of microns. In this section we demonstrate by means of a boundary-layer approximation that in the case  $\epsilon \ll 1$ , a sharp interface develops and the phase-field model reduces asymptotically to the free boundary mod-

el. The latter includes the Gibbs-Thompson relation as well as a linear kinetic term. In particular, we recover the relations between the macroscopic interfacial parameters, the capillary length and the kinetic coefficient, and the "microscopic" parameters  $\xi$  and  $\tau$ .

The range of values of the product  $\lambda\Delta$  is restricted by physical considerations. Small values of  $\lambda\Delta$  correspond to very small growth rates, which lead to equilibrium shapes. On the other hand, large values of  $\lambda\Delta$ , relative to the height of the barrier, do not describe a regime of two coexisting phases. Thus, only the range  $\epsilon \ll \lambda\Delta < 1$  is considered.

It is assumed that the dynamical process generates and preserves a boundary layer of thickness  $O(\epsilon)$  in which the phase  $\phi$  varies sharply. This boundary layer is located along the interface, which is defined to be the contour line  $\phi=0$ . The purpose of the boundary-layer approximation is to obtain a reduced problem for the macroscopic field  $u$ , with boundary conditions at the moving interface determined by the microscopic dynamics. The domain is separated into an *inner region*, a strip of thickness  $\delta_1(\epsilon)$  along the interface, and an *outer region*, the complement region on both sides of the interface. In the inner region, a local set of coordinates is used: The arc-length  $s$  along the interface and a stretched coordinate  $\rho = r/\epsilon$ , where  $r$  is the distance from the interface chosen positive in the disordered phase and negative in the ordered phase. Note that both  $s$  and  $r$  are functions of  $(x,y,t)$  and satisfy the following relations:

$$\lim_{r \rightarrow 0} \frac{\partial r}{\partial t} = -v(s,t), \quad (4.1)$$

$$\lim_{r \rightarrow 0} \nabla^2 r = \kappa(s,t), \quad (4.2)$$

and

$$\lim_{r \rightarrow 0} \frac{\partial s}{\partial t} = \int_0^s ds' \kappa(s',t) v(s',t), \quad (4.3)$$

where  $\kappa$  is the local curvature of the interface.

Let  $U(\rho,s,t) = u(\epsilon\rho,s,t)$  and  $\Phi(\rho,s,t) = \phi(\epsilon\rho,s,t)$  denote the fields in the inner region. The transformed phase-field equations in this region are

$$\frac{\partial^2 U}{\partial \rho^2} + \epsilon \left[ (\kappa + v) \frac{\partial U}{\partial \rho} + \frac{1}{2} v \frac{\partial \Phi}{\partial \rho} \right] + O(\epsilon^2) = 0, \quad (4.4)$$

$$\left[ \frac{\partial^2 \Phi}{\partial \rho^2} + v \frac{\partial \Phi}{\partial \rho} + g(\Phi) + \lambda U \right] + \epsilon \left[ \kappa \frac{\partial \Phi}{\partial \rho} - \frac{\partial \Phi}{\partial t} - \frac{\partial s}{\partial t} \frac{\partial \Phi}{\partial s} \right] + O(\epsilon^2) = 0. \quad (4.5)$$

The central assumption of the boundary-layer approximation is that the solutions can be expanded in a regular power series of  $\epsilon$ ,

$$u(x,y,t) = u_0(x,y,t) + \epsilon u_1(x,y,t) + \epsilon^2 u_2(x,y,t) + \dots, \quad (4.6)$$

$$\phi(x,y,t) = \phi_0(x,y,t) + \epsilon \phi_1(x,y,t) + \epsilon^2 \phi_2(x,y,t) + \dots, \quad (4.7)$$

$$U(\rho, s, t) = U_0(\rho, s, t) + \epsilon U_1(\rho, s, t) + \epsilon^2 U_2(\rho, s, t) + \dots, \quad (4.8)$$

$$\Phi(\rho, s, t) = \Phi_0(\rho, s, t) + \epsilon \Phi_1(\rho, s, t) + \epsilon^2 \Phi_2(\rho, s, t) + \dots. \quad (4.9)$$

Since the location and the shape of the interface are determined by the phase variable  $\phi$ , the dynamical functions  $v(s, t)$  and  $\kappa(s, t)$  must be expanded in power series as well. The velocity is by definition of order 1; thus

$$v(s, t) = v_0(s, t) + \epsilon v_1(s, t) + \epsilon^2 v_2(s, t) + \dots. \quad (4.10)$$

The appropriate expansion for the curvature cannot be identified directly from the equations. The choice of the leading order is motivated by results of numerical simulations of the model. It was seen that as  $\epsilon \rightarrow 0$ , the dynamical process generates patterns which become more “decorated” as  $\epsilon$  decreases, resulting in very large values of the curvature. The lower bound for the radius of curvature is the thickness of the interface; therefore,  $\kappa$  can be comparable to  $\epsilon^{-1}$ . Thus, the asymptotic expansion of  $\kappa$  is assumed to be

$$\kappa(s, t) = \epsilon^{-1} \kappa_0(s, t) + \kappa_1(s, t) + \epsilon \kappa_2(s, t) + \dots. \quad (4.11)$$

Note that the expansion of  $\kappa$  in Refs. 28–30 corresponds to  $\kappa_0 = 0$ , so that (4.11) is a generalization.

The inner and outer expansions are matched at the interface in the following way: In a boundary layer near the interface,  $\delta_1(\epsilon) \leq \rho \leq \delta_2(\epsilon)$ , the fields  $U(\rho, s, t)$  and  $\Phi(\rho, s, t)$  must be identical to the fields  $u(\epsilon\rho, s, t)$  and  $\phi(\epsilon\rho, s, t)$ , respectively (for a more rigorous treatment of this point, see Ref. 30). This requirement leads to the matching conditions

$O(1)$ :

$$\lim_{\rho \rightarrow \pm\infty} U_0 = \lim_{\epsilon\rho \rightarrow \pm 0} u_0. \quad (4.12)$$

$O(\epsilon)$ :

$$\lim_{\rho \rightarrow \pm\infty} \frac{\partial U_1}{\partial \rho} = \lim_{\epsilon\rho \rightarrow \pm 0} \frac{\partial u_0}{\partial r}, \quad (4.13)$$

$$\lim_{\rho \rightarrow \pm\infty} U_1 = \lim_{\epsilon\rho \rightarrow \pm 0} \left[ u_1 + \rho \frac{\partial u_0}{\partial r} \right]. \quad (4.14)$$

$O(\epsilon^2)$ :

$$\lim_{\rho \rightarrow \pm\infty} \frac{\partial U_2}{\partial \rho} = \lim_{\epsilon\rho \rightarrow \pm 0} \left[ \frac{\partial u_1}{\partial r} + \rho \frac{\partial^2 u_0}{\partial r^2} \right], \quad (4.15)$$

$$\lim_{\rho \rightarrow \pm\infty} U_2 = \lim_{\epsilon\rho \rightarrow \pm 0} \left[ u_2 + \rho \frac{\partial u_1}{\partial r} + \frac{1}{2} \rho^2 \frac{\partial^2 u_0}{\partial r^2} \right], \quad (4.16)$$

and so on.

The power series (4.6)–(4.11) are substituted into Eqs. (3.12) and (3.13) and Eqs. (4.4) and (4.5), respectively, subject to the matching conditions (4.12)–(4.16). The problem is then solved recursively. Since the inner and outer expansions are coupled by the matching conditions,

there is a continual feedback between the macroscopic and the microscopic levels. For the leading term we obtain the equations

$$\frac{\partial u_0}{\partial t} + \frac{1}{2} \frac{\partial \phi_0}{\partial t} = \nabla^2 u_0, \quad (4.17)$$

$$g(\phi_0) + \lambda u_0 = 0, \quad (4.18)$$

$$\frac{\partial^2 U_0}{\partial \rho^2} + \kappa_0 \frac{\partial U_0}{\partial \rho} = 0, \quad (4.19)$$

and

$$\frac{\partial^2 \Phi_0}{\partial \rho^2} + (v_0 + \kappa_0) \frac{\partial \Phi_0}{\partial \rho} + g(\Phi_0) + \lambda U_0 = 0. \quad (4.20)$$

From Eq. (4.18) it follows that  $\phi_0$  is the equilibrium value everywhere, i.e.,

$$\phi_0(x, y, t) = \begin{cases} \phi_+(u_0(x, y, t)) & \text{for } r(x, y, t) > 0 \\ \phi_-(u_0(x, y, t)) & \text{for } r(x, y, t) < 0. \end{cases} \quad (4.21)$$

It follows that  $u_0$  satisfies the diffusion equation

$$\left[ 1 + \frac{1}{2} \frac{\partial \phi_0}{\partial u_0} \right] \frac{\partial u_0}{\partial t} = \nabla^2 u_0. \quad (4.22)$$

For the case (3.3),  $\partial \phi_+ / \partial u = \partial \phi_- / \partial u = \lambda$ , so that (4.22) is a linear symmetric diffusion equation. Integrating Eq. (4.19) once and using the fact that  $U_0$  must be a bounded function of  $\rho$ , it is found that

$$U_0(\rho, s, t) = C_1(s, t), \quad (4.23)$$

where  $C_1(s, t)$  is the integration constant. Substituting (4.23) into Eq. (4.20), it is found that  $\Phi_0$  is the solution of

$$\frac{\partial^2 \Phi_0}{\partial \rho^2} + [v_0(s, t) + \kappa_0(s, t)] \frac{\partial \Phi_0}{\partial \rho} = -g(\Phi_0) - \lambda C_1(s, t), \quad (4.24)$$

subject to the boundary conditions

$$\lim_{\rho \rightarrow \pm\infty} \Phi_0(\rho, s, t) = \phi_{\pm}[C_1(s, t)]. \quad (4.25)$$

Equation (4.24), together with the boundary conditions (4.25), forms a nonlinear eigenvalue problem, which determines a relation between  $C_1$  and  $(v_0 + \kappa_0)$ . It is useful to consider the following mechanical analogy.<sup>27</sup> Equation (4.24) can also be viewed as the equation of motion of a particle, where  $\Phi_0$  plays the role of position and  $\rho$  corresponds to time. The particle moves in a potential field

$$V(\Phi_0) = - \int g(\Phi_0) d\Phi_0 - \lambda C_1 \Phi_0,$$

with a dissipation constant  $(v_0 + \kappa_0)$ . This potential field has the form of an *inverted* nonsymmetric double-well potential [see Fig. 4(a)]. The trajectory starts at “time”  $\rho = -\infty$  at the maximum “point”  $\Phi = \phi_-(C_1)$  and ends at time  $\rho = \infty$  at the second maximum point  $\Phi = \phi_+(C_1)$ . This trajectory corresponds to a homoclinic line in phase space [Fig. 4(b)]. In this analogous picture, it is clear that

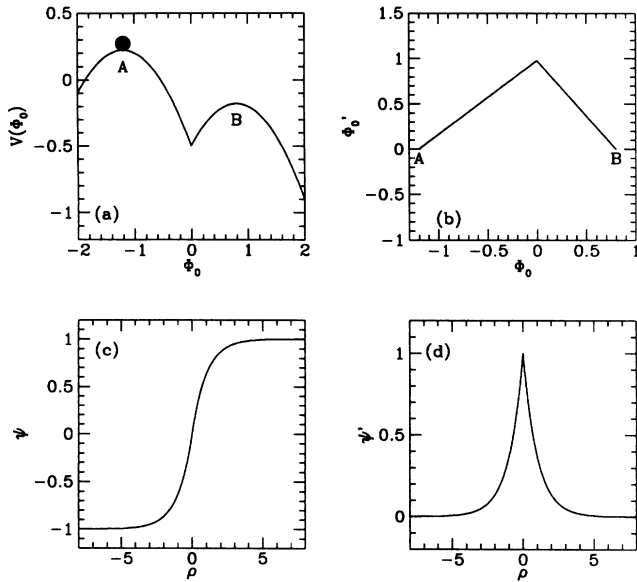


FIG. 4. The profile of the interface seen as an instanton. (a) The particle moves in the potential field,  $V(\phi)$ , starting its trajectory at  $A$  and ending it at  $B$ . (b) The homoclinic line in phase space  $\Phi_0(\phi_0)$ . (c) The equilibrium profile  $\psi(\rho)$  in real space. (d) The derivative of the profile,  $\psi'(\rho)$ .

there is a unique “dissipation coefficient,” for which such a trajectory exists. For  $\lambda C_1 < 1$ ,

$$C_1(s, t) \sim -d_0 \frac{\kappa_0(s, t)}{\epsilon} - \beta v_0(s, t), \quad (4.26)$$

where

$$d_0 = \frac{\epsilon}{2\lambda} \int_{-\infty}^{\infty} d\rho [\psi'(\rho)]^2 \quad (4.27)$$

and

$$\beta = \frac{1}{2\lambda} \int_{-\infty}^{\infty} d\rho [\psi'(\rho)]^2. \quad (4.28)$$

The function  $\psi(\rho)$  is the solution of Eq. (4.24) with  $C_1 = 0$  and is thus the equilibrium profile of the interface. The matching conditions of  $u_0$ , together with Eq. (4.26), imply that

$$\lim_{\epsilon \rightarrow \pm 0} u_0 = -d_0 \frac{\kappa_0(s, t)}{\epsilon} - \beta v_0(s, t). \quad (4.29)$$

The boundary condition (4.29) is exactly the one used in the free boundary model,<sup>4</sup> where it was introduced as an *ad hoc* correction. Here it appears as a rigorous reduction of microscopic dynamics. The capillary length  $d_0$  is the surface energy of the equilibrium profile of the interface, i.e., surface tension. In the mechanical analogy,  $d_0$  is the action of the trajectory or the integral of the kinetic energy along the trajectory. The constant  $\beta$  is the so-called surface kinetic coefficient and is simply proportional to surface tension  $\beta = d_0/\epsilon$ .

For the free energy (3.3),  $g(\phi) = \text{sgn}(\phi) - \phi$ , we find

$$\psi(\rho) = \text{sgn}(\rho) \{1 - \exp[-\text{sgn}(\rho)]\}. \quad (4.30)$$

Substituting into Eqs. (4.27) and (4.28), we obtain

$$d_0 = \frac{\epsilon}{2\lambda}, \quad \beta = \frac{1}{2\lambda}. \quad (4.31)$$

In dimensional units,  $d_0 = \xi/2\lambda$  and  $\beta = \tau/2\lambda\xi$ . For the case of the Ginzburg-Landau potential,  $g(\phi) = -\frac{1}{2}(\phi^3 - \phi)$ , we find  $d_0 = \xi/3\lambda$  and  $\beta = \tau/3\lambda\xi$ .

Equation (4.22) together with boundary condition (4.29) are not a complete set of equations for  $u_0$ . An additional boundary condition is obtained by considering the  $O(\epsilon)$  terms and applying matching conditions (4.13), yielding

$$\left. \frac{\partial u_0}{\partial r} \right|_{0^+} - \left. \frac{\partial u_0}{\partial r} \right|_{0^-} = -v_0(s, t). \quad (4.32)$$

Thus the free boundary model is a first approximation to the phase-field model in contrast to Refs. 28–30, where it is a second approximation, the first one being the Stefan problem.

## V. THE STEADY-STATE VELOCITY OF A FLAT INTERFACE: THE SOLVABILITY ANALYSIS

In this section we study the steady-state solution of a flat interface advancing with constant velocity. Such a solution was shown to exist in the free boundary model; therefore, its existence is expected in this model as well. In a moving frame of reference, Eqs. (3.12) and (3.13) take the form

$$\frac{\partial u}{\partial t} + \frac{1}{2} \frac{\partial \phi}{\partial t} = v \frac{\partial u}{\partial z} + \frac{1}{2} \frac{\partial \phi}{\partial z} + \nabla^2 u, \quad (5.1)$$

$$\epsilon \frac{\partial \phi}{\partial t} = \epsilon^2 \nabla^2 \phi + \epsilon v \frac{\partial \phi}{\partial z} - \phi + \text{sgn}(\phi) + \lambda u, \quad (5.2)$$

where  $z = x - vt$  and  $v$  is the velocity of the interface which is determined below from a solvability condition. The stationary solutions  $\phi_0(z), u_0(z)$  satisfy the equations

$$u_0'' + v u_0' + \frac{1}{2} v \phi_0' = 0, \quad (5.3)$$

$$\epsilon^2 \phi_0'' + \epsilon v \phi_0' - \phi_0 + \text{sgn}(\phi_0) + \lambda u_0 = 0 \quad (5.4)$$

(all derivatives are with respect to  $z$ ), subject to the boundary conditions

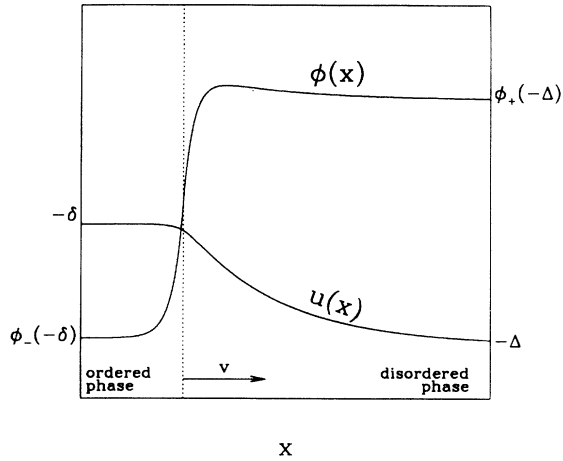
$$u_0(\infty) = -\Delta, \quad \phi_0(\infty) = \phi_+(\infty) = 1 - \lambda \Delta \quad (5.5)$$

and

$$u_0(-\infty) = -\delta, \quad \phi_0(-\infty) = \phi_-(-\delta) = -1 - \lambda \delta, \quad (5.6)$$

where  $\delta$  and  $\Delta$  are the values of  $u$  in the ordered and disordered phases, respectively, far from the interface. These are the most general boundary conditions providing that there are opposite phases on each side of the interface (see Fig. 5). As this problem has no explicit dependence on the  $z$  coordinate, the solution is invariant under translations along the  $z$  axis. The origin is set arbitrarily at

$$\phi_0(0) = 0. \quad (5.7)$$

FIG. 5. Steady-state profiles of  $\phi(x)$  and  $u(x)$ .

Integration of Eq. (5.3) results in

$$u'_0 + v u_0 + \frac{1}{2} v \phi_0 = C_1. \quad (5.8)$$

Substitute the boundary conditions (5.5) and (5.6) into Eq. (5.8), the integration constant is determined as

$$C_1 = v \left[ \frac{1}{2} - \Delta(1 + \lambda/2) \right],$$

and

$$\delta = \Delta - \frac{1}{1 + \lambda/2}. \quad (5.9)$$

Referring again to the example of a thermal field during solidification, this constraint is nothing but global energy conservation. It states that the amount of heat needed to raise the temperature from  $u = -\Delta$  to  $u = -\delta$  is equal to the amount of latent heat released during solidification. The driving force for which the ordered phase forms at equilibrium is defined as

$$\Delta_c = \frac{1}{1 + \lambda/2} \quad (5.10)$$

(it corresponds to  $\Delta = 1$  in solidification).

Combining Eqs. (5.4) and (5.8), a third-order equation is obtained:

$$\begin{aligned} \epsilon^2 \phi_0''' + \epsilon(\epsilon + 1)v \phi_0'' + (\epsilon v^2 - 1)\phi_0' - \frac{1}{\Delta_c} v \phi_0 \\ = -2\delta(z) - v \operatorname{sgn}(z) + \lambda v \left[ \frac{1}{2} + \frac{\delta}{\Delta_c} \right], \end{aligned} \quad (5.11)$$

with boundary conditions expressed in terms of  $\delta$  as

$$\phi_0(-\infty) = -1 - \lambda\delta, \quad \phi_0(\infty) = 1 - \lambda(\delta + \Delta_c). \quad (5.12)$$

Equation (5.11) is solved piecewise, imposing matching conditions at  $z = 0$ ,

$$\phi_0(0^+) = \phi_0(0^-) = 0, \quad (5.13)$$

$$\phi_0'(0^+) = \phi_0'(0^-), \quad (5.14)$$

and

$$\phi_0''(0^+) - \phi_0''(0^-) = -\frac{2}{\epsilon^2}, \quad (5.15)$$

the discontinuity of the second derivative resulting from  $\delta(z)$ . The solution to the homogeneous problem is a linear combination of exponential terms  $\exp(q_i z)$ , where  $q_i$  ( $i = 1, 2, 3$ ) are the solutions of the cubic equation

$$\epsilon^2 q^3 + \epsilon(\epsilon + 1)v q^2 + (\epsilon v^2 - 1)q - v/\Delta_c = 0. \quad (5.16)$$

We distinguish now between the two following cases:

*Case I.*  $\operatorname{Re}(q_1) > 0$ ,  $\operatorname{Re}(q_2) \geq 0$ , and  $\operatorname{Re}(q_3) < 0$ . The solution of Eq. (5.11) is

$$\phi_0(z) = \begin{cases} -(1 + \lambda\delta) + A \exp(q_1 z) + B \exp(q_2 z) & \text{if } z < 0 \\ 1 - \lambda(\delta + \Delta_c) + C \exp(q_3 z) & \text{if } z > 0. \end{cases} \quad (5.17)$$

Substituting the matching conditions (5.13)–(5.15), the solvability condition

$$(q_1 + q_2 - q_3)q_3 \left[ \delta\lambda - \frac{1 - \lambda/2}{1 + \lambda/2} \right] - q_1 q_2 (1 + \lambda\delta) = \frac{2}{\epsilon^2} \quad (5.18)$$

is obtained.

*Case II.*  $\operatorname{Re}(q_1) > 0$ ,  $\operatorname{Re}(q_2) \leq 0$ , and  $\operatorname{Re}(q_3) < 0$ . The solution of Eq. (5.11) is

$$\phi_0(z) = \begin{cases} -(1 + \lambda\delta) + D \exp(q_1 z) & \text{if } z < 0 \\ 1 - \lambda(\delta + \Delta_c) + E \exp(q_2 z) + F \exp(q_3 z), & \text{if } z > 0 \end{cases} \quad (5.19)$$

and the solvability condition is

$$(q_1 - q_2 - q_3)q_1(1 + \lambda\delta) + q_2 q_3 \left[ \delta\lambda - \frac{1 - \lambda/2}{1 + \lambda/2} \right] = \frac{2}{\epsilon^2}. \quad (5.20)$$

In order to find  $v(\delta)$ , we calculate the roots  $q_i$  from Eq. (5.16) for each  $v > 0$ ; then, according to the case, we extract  $\delta$  out of Eq. (5.18) or Eq. (5.20).

To check this result, we consider the limit of a sharp interface ( $\epsilon \ll 1$ ) and show that it reduces to the result of the free boundary model. Expand  $v$ ,  $q_i$ , and  $\delta$  as power series of  $\epsilon$ ,

$$v = v^{[0]} + \epsilon v^{[1]} + \dots, \quad (5.21)$$

$$q = \epsilon^{-1} q^{[0]} + q^{[1]} + \dots, \quad (5.22)$$

$$\delta = \delta^{[0]} + \epsilon \delta^{[1]} + \dots. \quad (5.23)$$

The three roots of Eq. (5.16) are

$$q_1 = \frac{1}{2\epsilon} \{ [(v^{[0]})^2 + 4]^{1/2} - v^{[0]} \} + \mathcal{O}(1),$$

$$q_2 = -\frac{1}{2\epsilon} \{ [(v^{[0]})^2 + 4]^{1/2} + v^{[0]} \} + \mathcal{O}(1), \quad (5.24)$$

$$q_3 = -\frac{v^{[0]}}{\Delta_c} + \mathcal{O}(\epsilon).$$

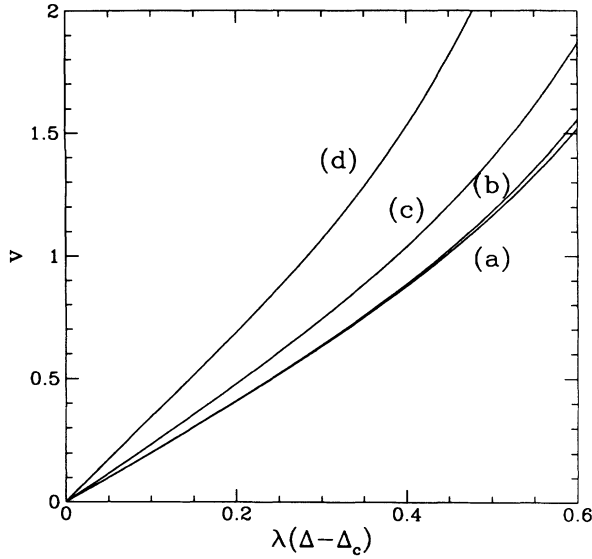


FIG. 6. Plots of  $v$  vs  $\lambda(\Delta - \Delta_c)$  for (a)  $\epsilon=0.01$  and  $\lambda=0.1$ , (b)  $\epsilon=0.01$  and  $\lambda=0.3$ , (c)  $\epsilon=1.0$  and  $\lambda=0.1$ , and (d)  $\epsilon=1.0$  and  $\lambda=0.3$ .

For small  $\epsilon$ , this corresponds to case II. Substituting Eqs. (5.23) and (5.24) in Eq. (5.20), we obtain

$$v^{[0]} \{ [(v^{[0]})^2 + 4]^{1/2} - v^{[0]} \} = \frac{2\lambda\delta^{[0]}}{1 + \lambda\delta^{[0]}}, \quad (5.25)$$

which for small  $\lambda\delta$  (and consequently, small  $v$ ) reduces to

$$v^{[0]} \approx 2\lambda\delta^{[0]}. \quad (5.26)$$

Comparing to Eq. (4.31), we identify the prefactor  $2\lambda$  as the inverse of the kinetic coefficient  $\beta^{-1}$ . We thus retrieve the result of the free boundary model,

$$v = \frac{1}{\beta} (\Delta - \Delta_c). \quad (5.27)$$

In Fig. 6 the plot  $v[\lambda(\Delta - \Delta_c)]$  is given for different values of  $\epsilon$  and  $\lambda$ . For  $\epsilon=0.01$ , it is found that the velocity is mainly a function of the product  $\lambda(\Delta - \Delta_c)$ , but for fixed  $\Delta - \Delta_c$  depends weakly on  $\lambda$ , in agreement with Eq. (5.27). The dependence is approximately linear for sufficiently small values of  $(\Delta - \Delta_c)$ . For  $\lambda(\Delta - \Delta_c) \rightarrow 1 - \lambda\Delta_c$ , the velocity grows sharply to infinity. This is due to the fact that for  $\lambda\Delta > 1$ , the potential is no longer a double well; thus, bistability is destroyed. This range of parameters is therefore of no interest for our purposes.

## VI. LINEAR STABILITY SPECTRUM OF A FLAT INTERFACE

In this section we develop the linear stability analysis of the steady-state solution of a flat interface, obtained in Sec. V. We study the time evolution of a small periodic perturbation added to the stationary solutions  $\phi_0(z)$  and  $u_0(z)$  of the form

$$\phi(z, y, t) = \phi_0(z) + \eta\phi_1(z)\exp(iky + \omega t), \quad (6.1)$$

$$u(z, y, t) = u_0(z) + \eta u_1(z)\exp(iky + \omega t),$$

where  $\eta \ll 1$ . Physically, we are interested only in perturbations which are initially localized near the interface. Thus, we require that  $\phi_1(z)$  and  $u_1(z)$  decay as  $z \rightarrow \pm\infty$ . We substitute Eq. (6.1) into the time-dependent equations (5.1) and (5.2) and linearize with respect to  $\eta$ , yielding

$$u_1'' + v u_1' + \frac{1}{2} v \phi_1' - (\omega + k^2) u_1 - \frac{1}{2} \omega \phi_1 = 0, \quad (6.2)$$

$$\epsilon^2 \phi_1'' + \epsilon v \phi_1' - (\epsilon\omega + \epsilon^2 k^2 + 1) \phi_1 + \lambda u_1 = -2\delta(\phi_0(z)) \phi_1. \quad (6.3)$$

The  $\delta$  function can be rewritten as

$$2\delta(\phi_0(z)) \phi_1 = 2 \frac{\phi_1(0)}{|\phi_0'(0)|} \delta(z), \quad (6.4)$$

while from Eqs. (5.17) and (5.19), it follows that

$$|\phi_0'(0)| \equiv \xi = \begin{cases} \left| q_3 \left[ \delta\lambda - \frac{1-\lambda/2}{1+\lambda/2} \right] \right| & \text{in case I} \\ |q_1(1+\delta\lambda)| & \text{in case II.} \end{cases} \quad (6.5)$$

This problem is a nonlinear eigenvalue problem for  $\omega$  (which is complex), as a function of the wave number  $k$ . For a given  $k$ , there is at most a discrete set of values of  $\omega$ , for which a solution exists.

Similarly to the method used in Sec. V, the homogeneous equations are solved in the two domains; then  $\omega(k)$  is found by imposing the matching conditions

$$\phi_1(0^+) - \phi_1(0^-) = 0, \quad (6.6)$$

$$u_1(0^+) - u_1(0^-) = 0, \quad (6.7)$$

$$\phi_1'(0^+) - \phi_1'(0^-) = -\frac{2\phi_1(0)}{\epsilon^2 \xi}, \quad (6.8)$$

and

$$u_1'(0^+) - u_1'(0^-) = 0. \quad (6.9)$$

The solution of Eqs. (6.2) and (6.3) is a linear combination of four exponential terms:

$$\phi_1(z) = \sum_{i=1}^4 B_i \exp(Q_i z) \quad (6.10)$$

and

$$u_1(z) = \sum_{i=1}^4 \pi_i B_i \exp(Q_i z), \quad (6.11)$$

where

$$\pi_i = -\frac{1}{\lambda} [\epsilon^2 Q_i^2 + \epsilon v Q_i - (\epsilon\omega + \epsilon^2 k^2 + 1)] \quad (6.12)$$

and the roots  $Q_i$  are the solutions of the quartic equation

$$\begin{aligned} \epsilon^2 Q^4 + [\epsilon(\epsilon+1)v] Q^3 + [\epsilon v^2 - \epsilon(\epsilon+1)\omega - 2\epsilon^2 k^2 - 1] Q^2 \\ + \{-v[2\epsilon\omega + \epsilon(\epsilon+1)k^2 + 1 + \lambda/2]\} Q \\ + [(\omega + k^2)(\epsilon\omega + \epsilon^2 k^2 + 1) + \lambda\omega/2] = 0. \end{aligned} \quad (6.13)$$

Given a value of  $k$ , the corresponding  $\omega$  is found in the complex plane. For any  $\omega$ , the four roots  $Q_i$  are calculated out from Eq. (6.13); then the following three cases are considered:

*Case I.*  $\text{Re}(Q_1) > 0$ ,  $\text{Re}(Q_2) \geq 0$ ,  $\text{Re}(Q_3) \leq 0$ , and  $\text{Re}(Q_4) < 0$ . Substituting the boundary and the matching conditions, a homogeneous set of linear equations is obtained; thus the following determinant must vanish:

$$D_I(\omega) = \begin{vmatrix} 1 & 1 & 1 & 1 \\ \pi_1 & \pi_2 & \pi_3 & \pi_4 \\ \pi_1 Q_1 & \pi_2 Q_2 & \pi_3 Q_3 & \pi_4 Q_4 \\ Q_1 - 2/\epsilon^2 \xi & Q_2 - 2/\epsilon^2 \xi & Q_3 & Q_4 \end{vmatrix} = 0. \quad (6.14)$$

*Case II.*  $\text{Re}(Q_1) > 0$ ,  $\text{Re}(Q_2) \geq 0$ ,  $\text{Re}(Q_3) \geq 0$ , and  $\text{Re}(Q_4) < 0$ . The vanishing determinant is

$$D_{II}(\omega) = \begin{vmatrix} 1 & 1 & 1 & 1 \\ \pi_1 & \pi_2 & \pi_3 & \pi_4 \\ \pi_1 Q_1 & \pi_2 Q_2 & \pi_3 Q_3 & \pi_4 Q_4 \\ Q_1 & Q_2 & Q_3 & Q_4 - 2/\epsilon^2 \xi \end{vmatrix} = 0. \quad (6.15)$$

*Case III.*  $\text{Re}(Q_1) > 0$ ,  $\text{Re}(Q_2) \leq 0$ ,  $\text{Re}(Q_3) \leq 0$ , and  $\text{Re}(Q_4) < 0$ . In this case, the vanishing determinant is

$$D_{III}(\omega) = \begin{vmatrix} 1 & 1 & 1 & 1 \\ \pi_1 & \pi_2 & \pi_3 & \pi_4 \\ \pi_1 Q_1 & \pi_2 Q_2 & \pi_3 Q_3 & \pi_4 Q_4 \\ Q_1 - 2/\epsilon^2 \xi & Q_2 & Q_3 & Q_4 \end{vmatrix} = 0. \quad (6.16)$$

If the real parts are either all nonpositive or all non-negative, there is no solution to the problem. Thus, the solvability condition is that the mismatch function

$$M(\omega) = \begin{cases} D_I(\omega) & \text{in case I} \\ D_{II}(\omega) & \text{in case II} \\ D_{III}(\omega) & \text{in case III} \\ \text{undefined} & \text{otherwise} \end{cases} \quad (6.17)$$

has to vanish. The stability spectrum is then found numerically.

As a first check of these results, the stability spectrum obtained by this procedure is compared to the stability spectrum calculated by the free boundary model (see the Appendix). The parameter  $d_0$  and  $\beta$  needed for the latter are evaluated using Eq. (4.31). In Fig. 7(a) ( $\epsilon=0.01$ ), the correspondence between the two results is excellent. In Fig. 7(b) ( $\epsilon=1.0$ ), where the approximation of the phase-field model by the free boundary model is expected to break, the correspondence between the two models is still very good. For example, the marginally stable mode deviates by only 5%, as seen in Fig. 7(b).

Next, the marginally stable mode  $k_{MS}$  is calculated as a function of the velocity (Fig. 8). For  $\epsilon=0.01$ ,  $k_{MS}$  is an increasing function of the driving force. The correspondence between the two models is excellent and breaks down only close to the degree of driving force where bi-

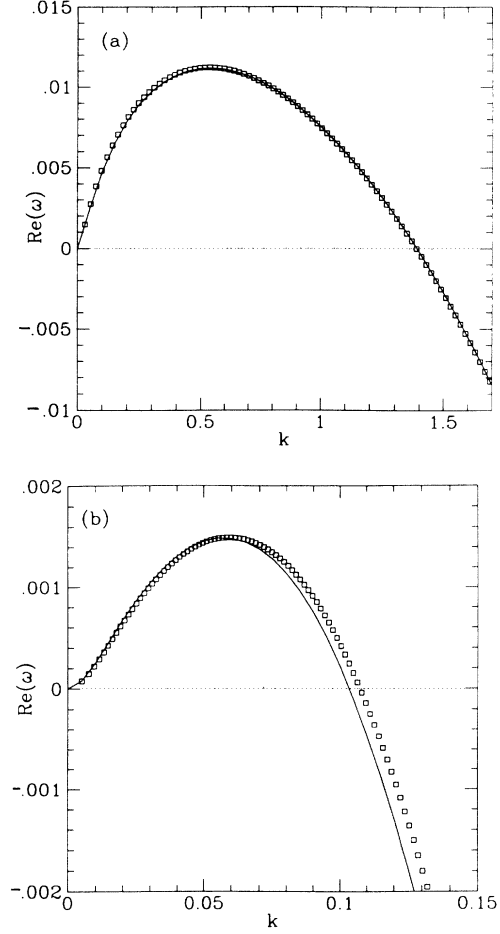


FIG. 7. Comparison between the stability spectrum obtained from the phase-field model (solid lines) and the free boundary model (dots). The parameters for the phase-field equations are  $\lambda=0.2$ ,  $\nu=0.1$ , and (a)  $\epsilon=0.01$ , (b)  $\epsilon=1.0$ .

stability is destroyed. For  $\epsilon=1.0$ , the result is completely different. It is found that  $k_{MS}$  attains a maximum before decreasing to zero. Above a critical driving force, there is no marginally stable mode, meaning that the interface is linearly stable with respect to perturbations of all wavelengths. The transition to the stable regime appears to occur when  $D/\nu$  becomes of order  $\xi$ . This behavior was pointed out for the free boundary model in Ref. 48. In this case the transition occurs when  $D/\nu$  becomes of the order of the capillary length  $d_0$ .

## VII. SUMMARY

We presented an analysis of a phase-field model defined by

$$\frac{\partial u}{\partial t} + \frac{1}{2} \frac{\partial \phi}{\partial t} = D \nabla^2 u \quad (7.1)$$

and

$$\tau \frac{\partial \phi}{\partial t} = \xi^2 \nabla^2 \phi + \text{sgn}(\phi) - \phi + \lambda u, \quad (7.2)$$

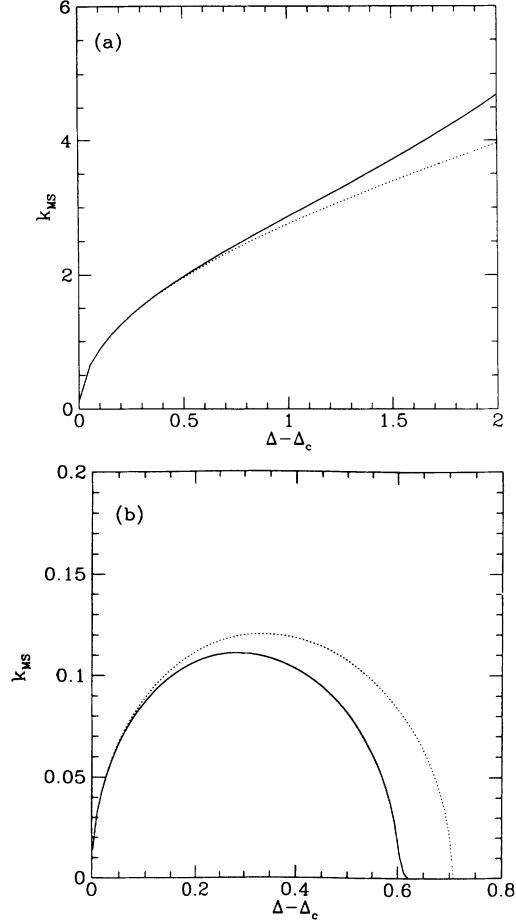


FIG. 8. The marginally stable mode  $k_{MS}$  as a function of the driving force  $\Delta - \Delta_c$ . Comparison between the phase-field model (solid line) and the free boundary model (dashed line). The parameters are  $\lambda = 0.2$  and (a)  $\epsilon = 0.01$ ; (b)  $\epsilon = 1.0$ .

with boundary conditions at  $|x| \rightarrow \infty$ ,  $u \rightarrow -\Delta$ , and  $\phi \rightarrow \phi_+(-\Delta)$ . In the limit  $\epsilon = \xi^2/D_\tau \ll 1$ , a sharp interface develops and the model reduces to leading order in  $\epsilon$  to the two-sided free boundary model given by

$$(1 + \frac{1}{2}\lambda) \frac{\partial u}{\partial t} = D \nabla^2 u, \quad (7.3)$$

with boundary conditions given on the moving interface,

$$D(\nabla_n u_+ - \nabla_n u_-) = -v \quad (7.4)$$

and

$$u_i = -d_0 \kappa - \beta v. \quad (7.5)$$

The interfacial parameters are related to the parameters of the phase-field model by

$$d_0 = \frac{\xi}{2\lambda}, \quad \beta = \frac{\tau}{2\lambda\xi}. \quad (7.6)$$

These results are essentially different from those presented in Refs. 28–30, where a different ansatz about the size of the curvature leads to an approximation of the interface by that of the Stefan problem. The effects of surface tension and surface kinetics enter as a second-order per-

turbation and are therefore negligible. The ansatz  $\kappa = O(1)$  is unrealistic because solutions of the Stefan problem with  $\kappa = O(1)$  are unstable and evolve in time to solutions with unbounded curvatures. In contrast, the ansatz  $\kappa = O(1/\epsilon)$  is self-consistent and holds for all times.

We presented a linear stability analysis about the steady-state solution of a planar interface. For  $\epsilon \ll 1$  the stability spectrum is in excellent agreement with the stability spectrum calculated for the free boundary model. For  $\epsilon \sim 1$ , the stability spectrum for both models is still in good agreement. In this limit, the interface becomes completely stable for driving forces above a critical value. The existence of a stable regime provides additional support to the hypothesis that the same dynamics can describe both the unstable growth of single realizations and stable growth of the ensemble averaged envelope. The stable growth regime is for the two fields having similar decay lengths, which is consistent with the observation in computer simulations of envelope dynamics.

Additional investigation of the phase-field model is required towards the modeling of the ensemble dynamics. In a subsequent article, we will extend the study to include surface anisotropy and show how anisotropy manifests as a singular effect when performing the boundary-layer approximation. Another issue for further study is the phase-field model for a conserved order parameter. It is still unclear whether the ensemble dynamics of single realizations described by a nonconserved field should be described by a conserved or nonconserved order parameter.

*Note added in proof.* After the submission of this paper, we became aware of closely related work by M. N. Barber and D. Singleton (unpublished).

#### ACKNOWLEDGMENTS

We are grateful to R. G. Mints, M. Ya. Azbel, D. Mukamel, H. Levine, W. Reynolds, and H. Müller-Krumbhaar for useful discussions. Parts of the results presented in Sec. II were obtained in collaboration with K. Kassner, H. Müller-Krumbhaar, and S. G. Lipson. This study was partly supported by a grant from the G.I.F., the German-Israeli Foundation for Scientific Research and Development, and by a grant from the University of Tel-Aviv.

#### APPENDIX: LINEAR STABILITY SPECTRUM FOR THE SYMMETRIC FREE BOUNDARY MODEL

In this appendix we derive the linear stability analysis for a steady-state planar interface for the free boundary model. In a frame of reference, moving with the interface at velocity  $v_0$ , the symmetric free boundary model is given by the system

$$\frac{\partial u}{\partial t} = \nabla^2 u + v_0 \frac{\partial u}{\partial z}, \quad (A1)$$

$$(v_0 + v_n) = -(\nabla_n u_+ - \nabla_n u_-), \quad (A2)$$

$$u_\infty = -\Delta, \quad u(-\infty) = -\delta, \quad (A3)$$

$$u_i = -d_0 \kappa - \beta(v_0 + v_n), \quad (A4)$$

where  $z = x - v_0 t$ . The stationary solution of a flat interface located at  $z = 0$ , is

$$u_0(z) = \begin{cases} -\beta v_0, & z < 0 \\ -\Delta + (\Delta - \beta v_0) \exp(-v_0 z), & z > 0. \end{cases} \quad (\text{A5})$$

Substituting into Eq. (A2), we obtain the relation between the velocity and the driving force  $\Delta$ ,

$$v_0 = \frac{1}{\beta} (\Delta - 1). \quad (\text{A6})$$

$$u(z, y, t) = \begin{cases} -\beta v_0 + \hat{u}_- \exp(iky + \omega t) \exp(q_- z), & z < 0 \\ -\Delta + (\Delta - \beta v_0) \exp(-v_0 z) + \hat{u}_+ \exp(iky + \omega t) \exp(-q_+ z), & z > 0 \end{cases} \quad (\text{A8})$$

where  $\hat{u}_-$  and  $\hat{u}_+$  are of order  $\hat{r}$ . Substituting into Eqs. (A1)–(A4) and linearizing with respect to the small parameters, we obtain

$$\omega = -k^2 + q_-^2 + v_0 q_-, \quad (\text{A9})$$

$$\omega = -k^2 + q_+^2 - v_0 q_+, \quad (\text{A10})$$

$$\omega = q_+ (-d_0 k^2 - \beta \omega + v_0) - v_0^2 - q_- (d_0 k^2 + \beta \omega). \quad (\text{A11})$$

By subtracting Eq. (A10) from Eq. (A9), one finds that  $q \equiv q_- = q_+ - v_0$ ; thus, we get  $\omega(k)$  in an implicit form:

$$\omega = \frac{v_0 q - d_0 k^2 (2q + v_0)}{1 + \beta (2q + v_0)} = -k^2 + q^2 + v_0 q. \quad (\text{A12})$$

To perform the linear stability analysis, we perturb the location of the interface in the  $z$  direction, denoted by  $r(y, t)$ . We consider the small periodic perturbation

$$r(y, t) = \hat{r} \exp(iky + \omega t), \quad (\text{A7})$$

where  $\hat{r} \ll 1$ , and calculate the amplification rate  $\omega$  as a function of  $k$ . The correction to  $u$ , due to perturbation of the interface, has the following form:

Next, we look for the marginally stable mode  $k_{MS}$  at which the amplification rate vanishes (besides  $k = 0$ , which is always a solution, the system being invariant under longitudinal translations). Substituting  $\omega = 0$  in Eq. (A12), we find

$$k_{MS} = \left[ \frac{v_0}{d_0} \right]^{1/2} \left\{ \frac{1}{8} [4 - p - (p^2 + 8p)^{1/2}] \right\}^{1/2}, \quad (\text{A13})$$

where  $p = v_0 d_0$  is the ratio of the capillary length  $d_0$  and the diffusion length  $1/v_0$ . As  $p \rightarrow 1$ , this expression vanishes. For  $p > 1$ , there is no real solution; hence,  $\omega(k)$  is nonpositive for all values of  $k$ . Thus, the interface is stable against perturbations of all wavelengths.

<sup>1</sup>D. A. Kessler, J. Koplik, and H. Levine, *Adv. Phys.* **37**, 255 (1988).

<sup>2</sup>J. S. Langer, *Science* **243**, 1150 (1989).

<sup>3</sup>E. Ben-Jacob and P. Garik, *Nature* **343**, 523 (1990).

<sup>4</sup>E. Ben-Jacob, N. Goldenfeld, J. S. Langer, and G. Schon, *Phys. Rev. Lett.* **51**, 1930 (1983).

<sup>5</sup>D. Kruskal and H. Segur, *Aeronautical Research Associates of Princeton Tech. Memo* **85**, 25 (1985).

<sup>6</sup>B. Caroli, C. Caroli, B. Roulet, and J. S. Langer, *Phys. Rev. A*

<sup>7</sup>M. Ben-Amar and B. Moussallam, *Physica D* **25**, 155 (1987).

<sup>8</sup>D. A. Kessler, J. Koplik, and H. Levine, *Phys. Rev. A* **33**, 3352 (1986).

<sup>9</sup>P. Pelce and Y. Pomeau, *Stud. Appl. Math.* **74**, 245 (1986).

<sup>10</sup>M. A. Lemieux, J. Liu, and G. Kotliar, *Phys. Rev. A* **36**, 1849 (1987).

<sup>11</sup>I. Meiron, *Phys. Rev. A* **33**, 2704 (1986).

<sup>12</sup>E. A. Brener and V. I. Melnikov, *Adv. Phys.* **40**, 53 (1991).

<sup>13</sup>E. Ben-Jacob, R. Godbey, N. D. Goldenfeld, J. Koplik, H. Levine, T. Mueller, and L. M. Sander, *Phys. Rev. Lett.* **55**, 1315 (1985).

<sup>14</sup>E. Ben-Jacob, P. Garik, T. Mueller, and D. Grier, *Phys. Rev. A* **38**, 1370 (1988).

<sup>15</sup>S. H. Tirmizi and W. N. Gill, *J. Cryst. Growth* **96**, 277 (1989).

<sup>16</sup>H. Honjo, S. Ohta, and M. Matsushita, *J. Phys. Soc. Jpn.* **55**, 2487 (1986).

<sup>17</sup>P. Oswald, J. Bechhoefer, and F. Melo, *Mater. Res. Bull.* **38** (1991).

<sup>18</sup>E. Ben-Jacob, P. Garik, and D. Grier, *Superlatt. Microstruct.*

**3**, 599 (1987).

<sup>19</sup>A. Dougherty, P. D. Kaplan, and J. P. Gollub, *Phys. Rev. Lett.* **58**, 1652 (1987).

<sup>20</sup>E. Ben-Jacob, G. Deutscher, P. Garik, N. Goldenfeld, and Y. Lareah, *Phys. Rev. Lett.* **57**, 1903 (1986).

<sup>21</sup>O. Shochet, K. Kassner, E. Ben-Jacob, S. G. Lipson, and H. Müller-Krumbhaar, *Physica A* **187**, 87 (1992).

<sup>22</sup>O. Shochet, R. Kupferman, and E. Ben-Jacob, in *Growth Patterns in Physical Sciences and Biology*, edited by E. Louis, L. M. Sander, P. Meakin, and J. M. Garcia-Ruiz (Plenum, New York, 1991).

<sup>23</sup>V. L. Ginzburg and L. D. Landau, *Zh. Eksp. Teor. Fiz.* **20**, 1064 (1950).

<sup>24</sup>P. C. Hohenberg and B. I. Halperin, *Rev. Mod. Phys.* **49**, 435 (1977).

<sup>25</sup>G. Caginalp and P. C. Fife, *Phys. Rev. B* **34**, 4940 (1986).

<sup>26</sup>J. B. Collins and H. Levine, *Phys. Rev. B* **31**, 6119 (1985).

<sup>27</sup>J. S. Langer, *Models of Pattern Formation in First-Order Phase Transitions* (World Scientific, Singapore, 1986).

<sup>28</sup>G. Caginalp and P. C. Fife, *Phys. Rev. B* **33**, 7792 (1986).

<sup>29</sup>G. Caginalp and P. C. Fife, *SIAM J. Appl. Math.* **48**, 506 (1986).

<sup>30</sup>P. C. Fife, *Dynamics of Internal Layers and Diffusive Interfaces* (Society for Industrial and Applied Mathematics, Philadelphia, 1988).

<sup>31</sup>F. Liu, M. Mondello, and N. Goldenfeld, *Phys. Rev. Lett.* **66**, 3071 (1991).

<sup>32</sup>G. J. Fix and J. T. Lin, *Nonlin. Anal. Theory Methods Appl.*

- 12, 811 (1988).
- <sup>33</sup>J. T. Lin, *I.M.A.J. Appl. Math.* **39**, 51 (1987).
- <sup>34</sup>R. Kobayashi (unpublished).
- <sup>35</sup>R. Kobayashi, in *Pattern Formation in Complex Dissipative Systems*, edited by S. Kai (World Scientific, Singapore, 1992).
- <sup>36</sup>Y. Saito, G. Goldbeck-Wood, and H. Müller-Krumbhaar, *Phys. Rev. Lett.* **58**, 1541 (1987).
- <sup>37</sup>H. Frahm, S. Ullah, and A. T. Dorsey, *Phys. Rev. Lett.* **66**, 3067 (1991).
- <sup>38</sup>O. Schochet, K. Kassner, E. Ben-Jacob, S. G. Lipson, and M. Müller-Krumbhaar, *Physica A* **181**, 136 (1992).
- <sup>39</sup>M. Ya. Azbel (unpublished).
- <sup>40</sup>H. Löwen and J. Bechhoefer, *Europhys. Lett.* **16**, 195 (1991).
- <sup>41</sup>O. Schochet, Master's thesis, Tel-Aviv University, 1992.
- <sup>42</sup>R. Kupferman, Master's thesis, Tel-Aviv University, 1991.
- <sup>43</sup>F. Liu and N. D. Goldenfeld, *Phys. Rev. A* **42**, 895 (1990).
- <sup>44</sup>M. Uwaha and Y. Saito, *Phys. Rev. A* **40**, 4716 (1989).
- <sup>45</sup>E. Brener, H. Levine, and Y. Tu, *Phys. Rev. Lett.* **66**, 1978 (1991).
- <sup>46</sup>D. A. Kessler, H. Levine, and W. N. Reynolds, *Phys. Rev. A* **42**, 6125 (1990).
- <sup>47</sup>E. M. Lifshits and L. P. Pitaevskii, *Physical Kinetics* (Pergamon, Oxford, 1981).
- <sup>48</sup>C. Misbah, D. Temkin, and H. Müller-Krumbhaar, *J. Phys.* **1**, 585 (1991).